

Received: 2020.03.18

Accepted: 2020.05.19

Available online: 2020.06.03

Published: 2020.07.30

# Fiber Type-Specific Morphological and Cellular Changes of Paraspinal Muscles in Patients with Severe Adolescent Idiopathic Scoliosis

Authors' Contribution:  
Study Design A  
Data Collection B  
Statistical Analysis C  
Data Interpretation D  
Manuscript Preparation E  
Literature Search F  
Funds Collection G

ABCEF 1 **Xiexiang Shao\***  
ABC 1 **Jian Chen\***  
ADFG 1 **Jingfan Yang\***  
BDFG 1 **Wenyuan Sui**  
BCEF 1 **Yaolong Deng**  
BCE 2 **Zifang Huang**  
ACEG 3 **Ping Hu**  
ABCDEG 1 **Junlin Yang**

1 Spine Center, Xin Hua Hospital Affiliated to Shanghai Jiao Tong University School of Medicine, Shanghai, P.R. China  
2 Department of Spine Surgery, Sun Yat-sen University First Affiliated Hospital, Guangzhou, Guangdong, P.R. China  
3 CAS, Center for Excellence in Molecular Cell Science, Shanghai, P.R. China

\* Xiexiang Shao, Jian Chen and Jingfan Yang are Co-first author

**Corresponding Authors:** Ping Hu, e-mail: [hup@sibcb.ac.cn](mailto:hup@sibcb.ac.cn), Junlin Yang, e-mail: [yjunlin@126.com](mailto:yjunlin@126.com), [yangjunlin@xinhumed.com.cn](mailto:yangjunlin@xinhumed.com.cn)

**Source of support:** This work was supported by the National Key Research and Development Program (2018YFC0116500) and the Key Project of Transformational Medicine Cross-Research Fund of Shanghai Jiaotong University (ZH2018ZDB04)

**Background:** Paraspinal muscle (PSM) has been suggested to have a role in adolescent idiopathic scoliosis (AIS). Few studies have investigated the fiber type-specific changes of PSM in detail.


**Material/Methods:** Bilateral multifidus muscles were harvested from the apical vertebra level (T7–T10) of 12 AIS patients and 6 control individuals. Immunohistological staining was performed to evaluate the muscle fiber type composition, fiber type-specific cross-sectional area (CSA), myonuclei density, and the total and activated satellite cell (SC) density. The correlations between these characteristics and curve initiation/severity were analyzed.

**Results:** In comparison with the PSM in convexity and the control group, PSM in concavity showed a significant reduction of CSA (concavity,  $2601.1 \pm 574.1 \mu\text{m}^2$ ; convexity,  $3732.1 \pm 545.1 \mu\text{m}^2$ ; control,  $3426.5 \pm 248.4 \mu\text{m}^2$ ), myonuclei density (concavity,  $2.0 \pm 0.3$  myonuclei/fiber; convexity,  $2.5 \pm 0.4$  myonuclei/fiber; control,  $2.2 \pm 0.2$  myonuclei/fiber), and activated SC density (concavity,  $0.7 \pm 0.4$  cells/100 fibers; convexity,  $1.5 \pm 0.7$  cells/100 fibers; control,  $1.2 \pm 0.3$  cells/100 fibers) for fiber type I. The Cobb angle was positively correlated with the bilateral ratio of CSA (convexity/concavity) for both fiber types. The apical vertebral translation was positively correlated with bilateral difference of myonuclei density (type I), total SC density (types I and II), and activated SC density (type I).

**Conclusions:** The fiber type-specific pathological changes on the concave side seemed to be more severe. Some fiber type-specific characteristics (CSA, myonuclei density, total/activated SC density) were closely associated with curve severity. More attention should be paid to PSM physiotherapy treatment on the concave side.

**MeSH Keywords:** **Biopsy • Fluorescent Antibody Technique • Paraspinal Muscles • Satellite Cells, Skeletal Muscle • Scoliosis**

**Full-text PDF:** <https://www.medscimonit.com/abstract/index/idArt/924415>

 3061

 4

 4

 28



## Background

Adolescent idiopathic scoliosis (AIS) is a 3-dimensional spinal deformity with Cobb angle  $\geq 10^\circ$  [1]. As a common pediatric musculoskeletal disorder, it begins in early puberty and affects 1–4% of adolescents [2]. Scoliosis curve progresses in two-thirds of patients during puberty, and adults with large curves ( $>40^\circ$ ) are more likely to continue to deteriorate [3]. Therefore, great attention is paid to restricting the curve progression before an individual with AIS reaches adulthood. However, there is still an incomplete understanding of the initiation and progression of AIS [1, 4].

Paraspinal muscle (PSM) plays a significant role in stabilizing the spine, and it has been suggested as having a role in AIS [2]. In recent decades, there have been multiple reports of bilateral PSM asymmetry [2,5–11]. Abnormal hyperintense signal of PSM has been identified on the concave side by magnetic resonance imaging [2,11], which was consistent with the histologic finding of increased fibrosis and fatty infiltration on concavity [6, 9]. Increased electrical activity of PSM was also found on the convex side [8,10]. In addition, it has been widely reported that the convex side has a higher numerical distribution of muscle fiber type I [8,12,13]. However, limited studies have determined the side of abnormality based on a strict control group and correlated the changes with curve severity [2,8], and the in-depth pathological changes of PSM in AIS remain incompletely known.

To our knowledge, few studies have investigated the morphological and cellular changes of PSM specific to the muscle fiber type. Physiologically, the type I fiber is more resistant to fatigue and primarily provides sustained contraction, while the type II fiber is involved in powerful bursts of activity [14]. Type I fiber plays a critical role in contributing to the tonic function for trunk postural control, which can be highly associated with scoliosis [8,15]. Therefore, knowledge of bilateral changes specific to the fiber type within PSM in AIS can provide valuable information to deeply understand the etiopathogenesis and potentially improve AIS treatment strategies to restore the function of the involved side.

The current study was performed to evaluate the underlying morphological (cross-sectional area [CSA] and proportion) and cellular changes (myonuclei density, total and activated satellite cell density) of the PSM specific to fiber type in AIS and to explore the relationship between these changes and curve initiation and severity. We hypothesized that there would be significant PSM fiber type-specific pathological changes on the concave side of AIS compared with contralateral (convex) side and healthy controls. We additionally hypothesized that bilateral differences of some fiber type-specific characteristics would be closely associated with curve initiation and severity.

## Material and Methods

### Participants

This study was performed according to the Declaration of Helsinki and under approval by the ethics committee at our local institution (No. XHEC-D-2019-093). The detailed inclusion criteria for AIS group were (1) AIS diagnosis and treatment with corrective surgical procedures between April 2019 and October 2019, and (2) major thoracic curve with apical vertebrae from T7 to T10. In addition, the detailed inclusion criteria for control group were: (1) aged from 10 to 18 years old, and (2) underwent spinal surgery for thoracic cancer or fracture from T7 to T10 between April 2019 and October 2019. Participants who were reluctant to join the study or declined to provide informed consent were excluded. Finally, we included a total of 12 consecutive eligible AIS subjects (10 females and 2 males, mean age  $14.8 \pm 4.0$  years) and 6 age-matched individuals (5 females and 1 male, mean age  $13.2 \pm 3.1$  years). The concave side for all individuals in the AIS group was the left side. The demographic data of AIS and control individuals are presented in Table 1.

### Radiographic data collection

For patients with AIS, standardized anteroposterior erect full-length spine radiographs were collected. Cobb angle was used to describe the degree of side-to-side thoracic spinal curvature [4]. The vertebral rotation of the thoracic apical vertebra was determined by the Nash and Moe method (from grade 0 to grade 4), while the Risser sign was used to measure the range of skeletal maturity by the degree of the iliac apophysis ossification (from grade 0 to grade 5) [4,16]. In addition, we also measured the thoracic apical vertebral translation (AVT, distance between the midpoint of C7 plumb line and the center of the thoracic apical vertebra), and the coronal balance (CB, distance between C7 plumb line and midline of sacrum) (Table 2) [11].

### Muscle biopsies

Bilateral thoracic multifidus muscles were harvested from the level of apical vertebra at the main thoracic curve (T7–T10) for AIS and same vertebral level region for the control group during surgery. After drying excess blood in muscle samples and removing visible fat/connective tissue, muscle tissues were mounted in frozen section medium (Thermo, 6520, USA) and immersed in isopentane cooled by liquid nitrogen [17]. The muscle biopsies were kept at  $-80^\circ\text{C}$  for subsequent histological analysis.

### Muscle immunohistological staining

A cryostat (Leica, CM1860) was used at  $-20^\circ\text{C}$  to obtain 10- $\mu\text{m}$  cryosections of cross-sectional muscle biopsy samples, and the sections were mounted on glass slides for further

**Table 1.** Demographic data of adolescent idiopathic scoliosis (AIS) and control groups.

	AIS	Control	P value
Sex			
Female	10 (83.3)	5 (83.3)	0.755
Male	2 (16.7)	1 (16.7)	
Age at surgery, y	14.8±4.0	13.2±3.1	0.486
Age at scoliosis initiation, y	12.1±1.7	N/A	
Side of main thoracic curve, left/right	0/12	N/A	
Height, cm	161.1±8.4	159.5±8.0	0.707
Weight, kg	48.0±7.8	49.5±5.2	0.678
BMI, kg/m <sup>2</sup>	18.4±1.8	19.5±1.5	0.239

Quantitative data are described as mean±standard deviation, and qualitative data are expressed as n (%). N/A – not applicable.

**Table 2.** Measured clinical/postural index for patients.

Patient	Cobb angle, degrees	AVT, cm	CB, cm	Vertebral rotation, degree 0-4	Risser sign, degree 0-5
1	40	3	3	2	4
2	41	3	1	1	1
3	48	5	1	1	5
4	55	5	-2	2	3
5	60	4	0	1	2
6	60	4	2	2	2
7	64	5	0	2	1
8	65	6	-1	1	4
9	67	10	3	3	3
10	74	5	3	1	0
11	80	4	-1	2	3
12	95	4	2	2	1

AVT – apical vertebrae translation; CB – coronal balance, absolute value <2 cm was considered neutral balance. The vertebral rotation was determined by the Nash and Moe method. The range of skeletal maturity was evaluate by the Risser sign according to the degree of the iliac apophysis ossification [4,16].

immunohistological staining. Muscle sections were fixed with 4% paraformaldehyde and permeabilized by 0.5% Triton X-100. For Pax7 staining, the sections were demasked by 0.01 M citric acid treatment at 95°C for 5 min before blocking. Then 1% bovine serum albumin (HyClone) was used to block the sections for 1 h at room temperature. Anti-laminin (Abcam, ab11575, 1: 500), anti-laminin 2 alpha (Abcam, ab11576, 1: 300), anti-fast myosin skeletal heavy chain (Abcam, ab91506, 1: 500), anti-Pax7 (Developmental Studies Hybridoma Bank, 1: 100), and anti-MyoD (BD Pharmingen, 554130, 1: 300) were selected

as primary antibodies for different staining strategies. Sections were incubated in primary antibodies overnight at 4°C and incubated in appropriate Alexa 488- or Alexa 594-labeled anti-mouse, anti-rabbit, or anti-rat secondary antibodies (Invitrogen, 1: 1000) for 1 h at room temperature. The nuclei were then stained with 4,6-diamidino-2-phenylindole (DAPI), and sections were coverslipped with antifade mounting media (Vector Laboratories, H-100).

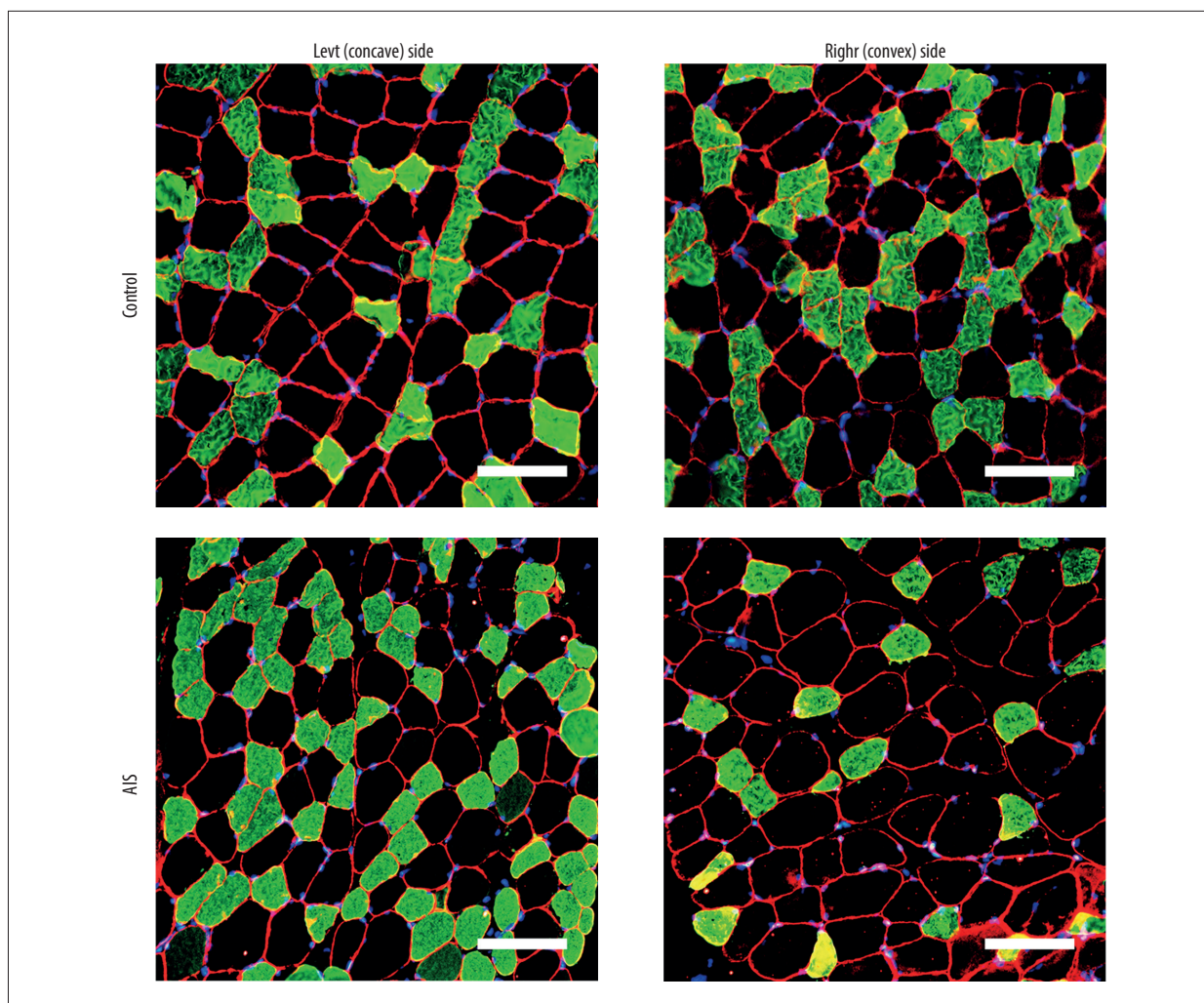


**Figure 1.** Representative bilateral paraspinal muscle immunohistological images of laminin 2 alpha (red), fast myosin skeletal heavy chain (green), and DAPI (blue) from individuals with adolescent idiopathic scoliosis and control individuals. The cross-sectional area is surrounded by laminin border. Muscle fiber type II can be stained with green while fiber type I cannot. Myonuclei were determined by DAPI<sup>+</sup> cells within the laminin border. Scale bar=100  $\mu$ m.

Fiber type composition and fiber type-specific CSA were evaluated by staining of fast myosin skeletal heavy chain, laminin 2 alpha, and DAPI (Figure 1). CSA was quantitatively analyzed by using Image Pro Plus software (Media Cybernetics). Total satellite cells (SCs) were identified by Pax7<sup>+</sup>/DAPI<sup>+</sup> cells within the laminin border (Figure 2) and activated SCs were assessed by MyoD<sup>+</sup>/DAPI<sup>+</sup> cells within the laminin border [17,18]. In addition, myonuclei were determined by DAPI<sup>+</sup> cells within the laminin border, while Pax7<sup>+</sup> nuclei were excluded from the myonuclei count. All the images were acquired by fluorescence microscope (Olympus, BX53) at  $\times 20$  magnification. Images were analyzed in a blinded manner, with the evaluator not knowing if the image was from the AIS or control group.

To facilitate the correlation test of clinical data with fiber type-specific characteristics, some parameters were explained as follows:

Bilateral ratio of fiber specific CSA=(fiber type-specific CSA<sub>convexity</sub>)/(fiber type-specific CSA<sub>concavity</sub>)

The difference of fiber type specific parameters=fiber type-specific parameter<sub>convexity</sub>-fiber type-specific parameter<sub>concavity</sub>

#### Statistical analysis

Statistical analysis was performed by SPSS version 19.0 for Windows (SPSS Inc., Chicago, IL, USA). The normality of continuous data was analyzed by the Shapiro-Wilk test. Multivariate analysis of variance (MANOVA) was performed



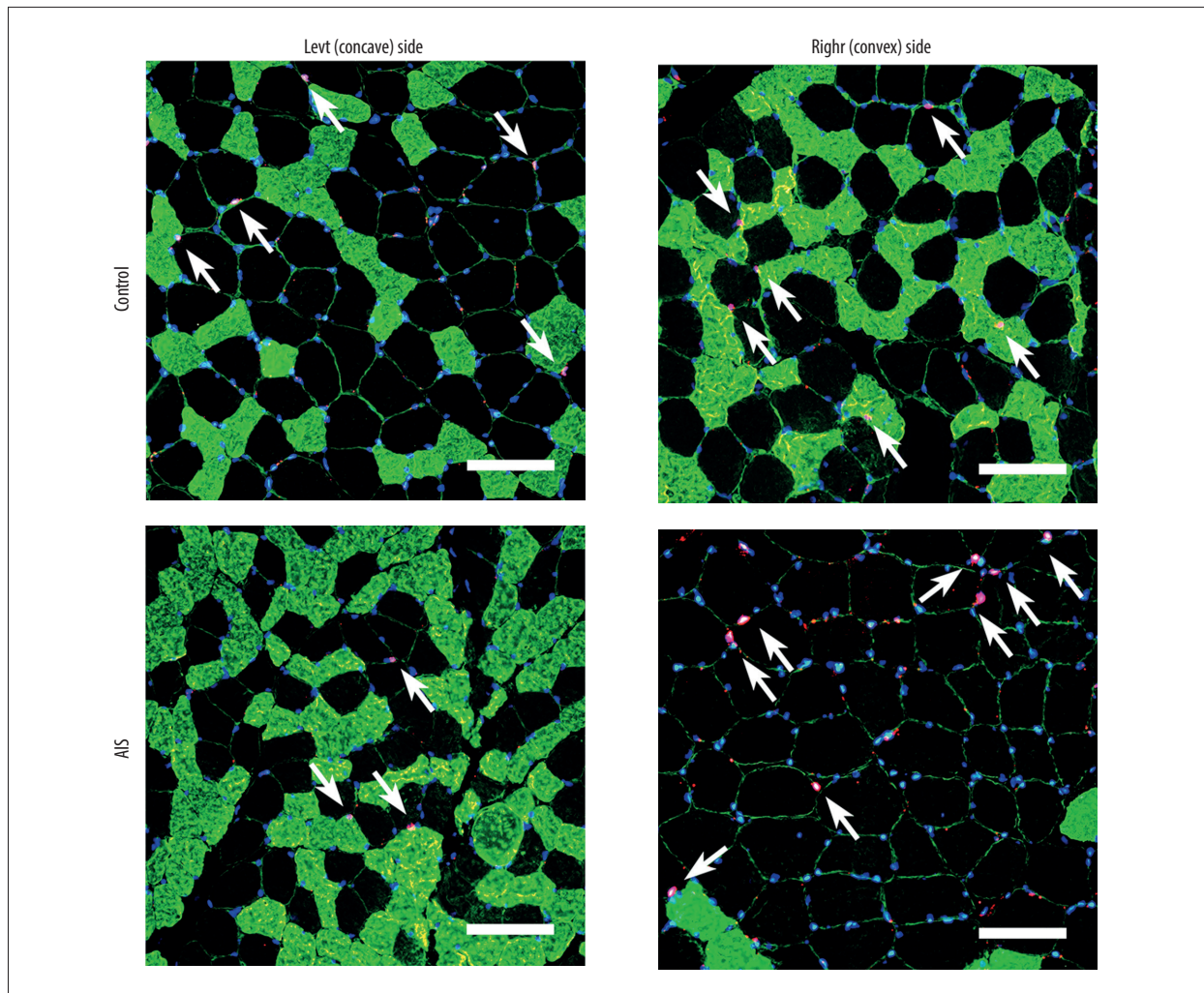


**Figure 2.** Representative bilateral paraspinal muscle immunohistological images of Pax7 (red), laminin (green), fast myosin skeletal heavy chain (green), and DAPI (blue) from individuals with adolescent idiopathic scoliosis and control individuals. Muscle fiber type II can be stained with green while fiber type I cannot. Satellite cells were identified by Pax7<sup>+</sup>/DAPI<sup>+</sup> cells within the laminin border. White arrows denote satellite cells (Pax 7<sup>+</sup>/DAPI<sup>+</sup>). Scale bar=100  $\mu$ m.

for between-group comparison (concave side in AIS versus left side in control, convex side in AIS versus right side in control), and GLM (repeated measure analysis of variance) was performed for the within-group comparisons. All the continuous data were normally distributed, except AVT and the age at initiation, so the correlations between clinical data (age at initiation, Cobb angle, AVT, CB) and bilateral difference of fiber type-specific characteristics were determined with Spearman or Pearson correlation analysis where applicable. Differences were considered significant with  $P < 0.05$ . Data are presented as mean  $\pm$  standard deviation.

## Results

### Muscle sample profile

At least 5 random fields were selected for each analysis of morphological and cellular characteristics. There were  $426.0 \pm 89.5$  fibers analyzed in the AIS group and  $377.3 \pm 73.1$  fibers analyzed in the control group for fiber type composition and CSA;  $420.7 \pm 99.9$  fibers analyzed in the AIS group and  $344.8 \pm 92.3$  fibers analyzed in control group for myonuclei and Pax7<sup>+</sup> cell counts; and  $435.2 \pm 128.0$  fibers analyzed in AIS group and  $473.8 \pm 90.0$  fibers analyzed in control group for the MyoD<sup>+</sup> cell counts.

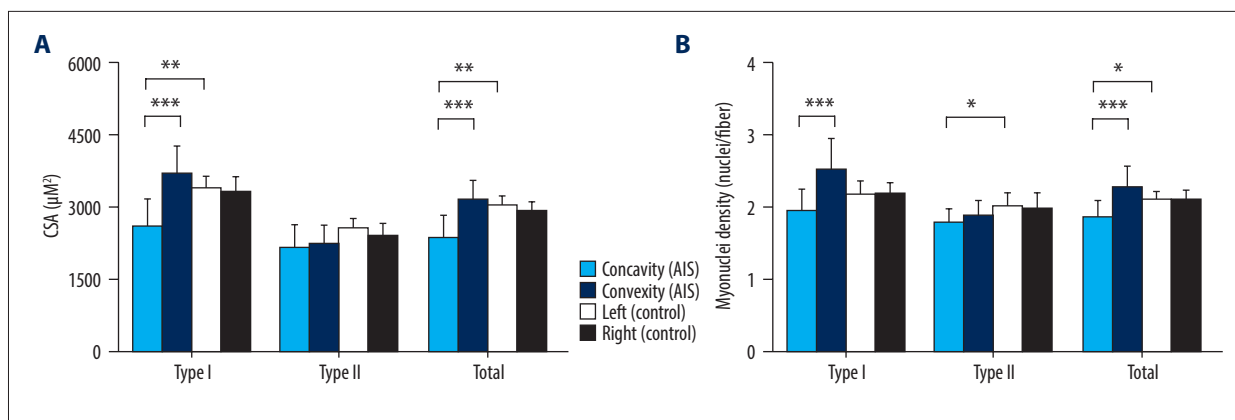


**Figure 3.** Fiber type specific cross-sectional area (A) and myonuclei density (B) from individuals with adolescent idiopathic scoliosis and control individuals. Data are presented as mean±SD. \*  $P<0.05$ , \*\*  $P<0.01$ , \*\*\*  $P<0.001$ . CSA – cross-sectional area.

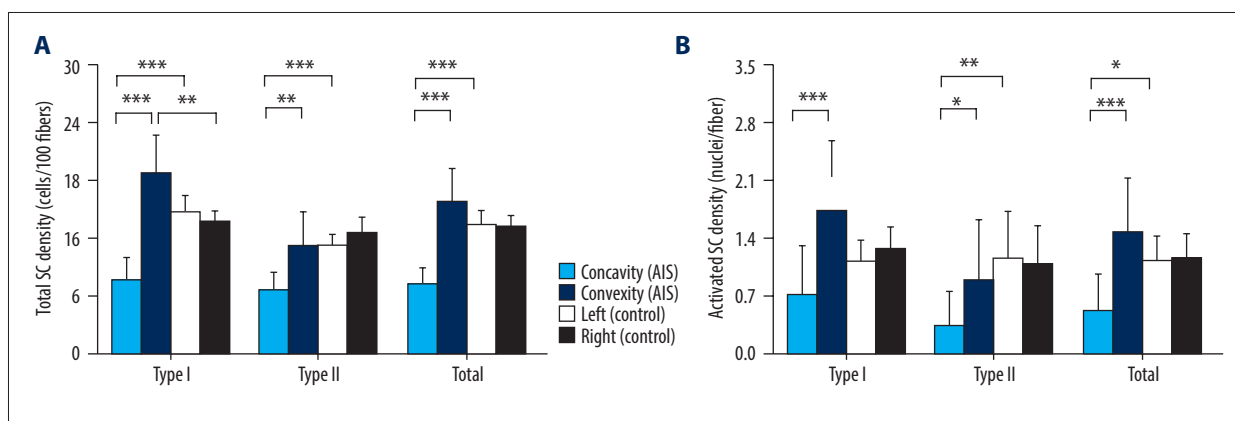


**Figure 4.** Fiber type specific total satellite cell density (A) and activated satellite cell density (B) from individuals with adolescent idiopathic scoliosis and control individuals. Data are presented as mean±SD. \*  $P<0.05$ , \*\*  $P<0.01$ , \*\*\*  $P<0.001$ . SC – satellite cell.

For the control group, no significant difference was found between the bilateral muscle fiber type-specific CSA, myonuclei density, and total and activated SC density (Figures 3, 4).

### Muscle fiber type composition and fiber size

The muscle fiber type composition of participants is detailed in Table 3. For the control group, the numerical proportion of type I fiber was significantly higher on the left side than the right side ( $P=0.001$ ), while the numerical proportion of type II fiber was significantly higher on the right side ( $P=0.001$ ). For the AIS group, patients showed  $12.1\pm 5.6\%$  higher numerical proportion and  $18.2\pm 5.6\%$  higher area proportion of type I fiber on the convex side than on the concave side.

For type I fiber, there was significant atrophy in concavity ( $2601.1\pm 574 \mu\text{m}^2$ ;  $P<0.001$  vs. convex side,  $P=0.005$  vs. left side of control). The concave side showed significant atrophy ( $2391.2\pm 449.5 \mu\text{m}^2$ ,  $P<0.001$  vs. convexity,  $P=0.005$  vs. left side of control) for total fiber types (Figure 3).

### Myonuclei density

Myonuclei in type I fiber were decreased in concavity ( $2.0\pm 0.3$  nuclei/fiber;  $P<0.001$  vs. convex side,  $P=0.108$  vs. left side of control). In addition, type II myonuclei on the concave side ( $1.8\pm 0.2$  nuclei/fiber) were also decreased ( $P=0.027$  vs. left side of control), which was similar with total fibers on the same side ( $1.9\pm 0.2$  nuclei/fiber;  $P<0.001$  vs. convex side,  $P=0.016$  vs. left side of control) (Figure 3).

### Total SC density

The total SC density in type I fiber was abnormally reduced on the concave side ( $7.8\pm 2.2$  cells/100 fibers;  $P<0.001$  vs. convexity side,  $P<0.001$  vs. left side of control) and increased on the convex side ( $19.1\pm 3.7$  cells/100 fibers;  $P<0.001$  vs. concavity side,  $P=0.007$  vs. right side of control). In type II fiber, the total SC density was found to be significantly decreased only in concavity ( $6.9\pm 1.7$  cells/100 fibers;  $P=0.001$  vs. convexity,  $P<0.001$  vs. left side of control). For total fiber types, fewer SCs

**Table 3.** Fiber type composition.

		Numerical proportion of Type I, %	Numerical proportion of Type II, %	Area proportion of Type I, %	Area proportion of Type II, %
AIS	Concavity	50.1±9.6	49.9±9.6	54.2±10.2	45.8±10.2
	Convexity	62.2±8.1	37.8±8.1	72.5±7.9	27.5±7.9
	<i>P</i> value	<0.001	<0.001	<0.001	<0.001
Control	Left side	57.8±4.1	42.2±4.1	64.8±3.4	35.2±3.4
	Right side	55.1±4.0	44.9±4.0	62.8±4.0	37.2±4.0
	<i>P</i> value	0.001	0.001	0.073	0.073

Quantitative data are described as mean±standard deviation.

**Table 4.** Correlation analysis between clinical parameters and the bilateral differences of fiber type specific morphological/cellular characteristics.

	Age at initiation		Cobb angle		AVT		CB	
	<i>r</i>	<i>P</i> value	<i>r</i>	<i>P</i> value	<i>r</i>	<i>P</i> value	<i>r</i>	<i>P</i> value
Difference of type I numerical proportion	-0.120	0.711	-0.002	0.996	-0.494	0.103	-0.167	0.603
Difference of type I area proportion	-0.198	0.537	-0.061	0.850	-0.182	0.571	0.091	0.779
Ratio of CSA								
Type I	0.004	0.991	<b>0.658</b>	<b>0.020*</b>	0.497	0.100	0.040	0.901
Type II	-0.172	0.593	<b>0.675</b>	<b>0.016*</b>	0.322	0.307	-0.269	0.398
Total	0.007	0.982	<b>0.737</b>	<b>0.006*</b>	0.438	0.155	-0.180	0.576
Difference of myonuclei density								
Type I	-0.071	0.826	0.302	0.341	<b>0.599</b>	<b>0.040*</b>	-0.150	0.641
Type II	0.108	0.737	-0.175	0.587	-0.133	0.680	-0.329	0.297
Total	0.093	0.773	0.326	0.301	0.571	0.053	-0.349	0.266
Difference of total SC density								
Type I	-0.228	0.476	0.351	0.263	<b>0.687</b>	<b>0.014*</b>	0.465	0.127
Type II	0.150	0.643	0.266	0.403	<b>0.680</b>	<b>0.015*</b>	0.088	0.787
Total	-0.019	0.954	0.346	0.271	0.539	0.070	0.328	0.297
Difference of activated SC density								
Type I	-0.116	0.720	0.495	0.102	<b>0.743</b>	<b>0.006*</b>	0.053	0.870
Type II	0.225	0.482	0.269	0.399	-0.025	0.940	-0.523	0.081
Total	-0.064	0.844	0.575	0.050	0.392	0.207	-0.427	0.166

AVT – apical vertebrae translation; CB – coronal balance; CSA – cross sectional area; SC – satellite cell. \* Significant if *P* value <0.05; the corresponding *P* and *r* values are bolded.

existed on the concave side ( $7.4 \pm 1.8$  cells/100 fibers;  $P < 0.001$  vs. convexity side,  $P < 0.001$  vs. left side of control) (Figure 4).

### Activated SC density

The number of activated SCs was consistently decreased on the concave side for type I ( $0.7 \pm 0.6$  cells/100 fibers;  $P < 0.001$  vs. convex side,  $P = 0.147$  vs. left side of control), type II ( $0.4 \pm 0.4$  cells/100 fibers;  $P = 0.013$  vs. convex side,  $P = 0.004$  vs. left side of control) and total fibers ( $0.6 \pm 0.4$  cells/100 fibers;  $P < 0.001$  vs. convex side,  $P = 0.01$  vs. left side of control) (Figure 4).

### Correlation analysis between clinical data and morphological/cellular characteristics

The results of the correlation analysis between the clinical data and the bilateral differences in morphological/cellular characteristics are presented in Table 4. Cobb angle was found to be significantly correlated with the bilateral ratio of CSA for type I ( $r = 0.658$ ,  $P = 0.020$ ), type II ( $r = 0.675$ ,  $P = 0.016$ ), and total fiber types ( $r = 0.737$ ,  $P = 0.006$ ). In addition, AVT was positively correlated with the bilateral difference of myonuclei density in fiber type I ( $r = 0.599$ ,  $P = 0.04$ ), as well as the bilateral difference of total SC density in fiber type I ( $r = 0.687$ ,  $P = 0.014$ ) and type II ( $r = 0.680$ ,  $P = 0.015$ ). Moreover, a positive correlation was also determined between AVT and the bilateral difference of activated SC density in fiber type I ( $r = 0.743$ ,  $P = 0.006$ ) (Table 4).

## Discussion

The current study evaluated bilateral fiber type-specific changes of PSM, including fiber type composition, CSA, myonuclei density, total SC density and activated SC density, in AIS compared with a control group. The results confirmed our hypotheses that there were significant PSM fiber type-specific pathological changes on the concave side of AIS compared with contralateral (convex) side and healthy controls. In addition, the bilateral differences of some fiber type-specific characteristics were closely associated with curve initiation and severity.

PSM plays a significant role in spine stability and postural control, and some investigators have suggested that the muscle plays a significant role in the initiation and progression of AIS [2,8]. In recent decades, bilateral PSM asymmetry in AIS has been widely discussed in terms of histology [8,12,13], muscle morphology [2,11], molecular biology [7], and biomechanical characteristics [5]. In particular, many studies have focused on the pathological changes of muscle fiber type-specific characteristics, revealing a numerical predominance of muscle fiber type I on the convex side [8,12,13]. Physiologically, the sustained and slow contractions of PSM are primarily provided by fatigue-resistant fiber type I, while the type II fibers fatigue

faster and provide powerful bursts of activity [14]. Considering the function of PSM in trunk postural control, detailed understanding of muscle fiber type-specific changes in PSM could help to elucidate the pathological mechanisms underlying AIS [8,15]. However, few studies have undertaken detailed investigation of fiber type-specific pathological changes of PSM, such as CSA, myonuclei density, and muscle SC characteristics.

Our finding of increased numerical proportions of type I fiber on convexity and type II fiber on concavity was consistent with a previous study [8]. In addition, the proportions of fiber type-specific areas also changed similarly to the numerical proportions. As for the CSA of muscle fibers, fiber type I on the concave side showed significant atrophy compared with the convex side and the control. Furthermore, the amount of myonuclei, a key predictor of muscle fiber size, also demonstrated consistent changes with CSA [17,19]. Previously, the size of muscle fiber was quantitatively analyzed by Mannion et al. [12], who found only bilateral type II atrophy. However, the parameter they used (narrow diameter) and nonstringent control sample (erector spinae vs. multifidus muscle) could have contributed to biased results [12]. Thus, as the first study to evaluate the fiber size by CSA and myonuclei content in AIS, the current result of fiber morphological change seems to be more reliable.

Muscle SCs play a critical role in skeletal muscle development and regeneration, which undergo high demanded with the pubertal growth spurt [20]. SCs remain quiescent until activation is invoked by microenvironment changes, which is followed by proliferation and differentiation. Both quiescent and activated SCs express Pax7, while MyoD is expressed in activated SCs [17,18]. In the current study, significantly reduced total and activated SCs were observed in concavity, indicating possible muscular degeneration and fiber atrophy [21]. However, there were significant increases of SCs on the convexity for type I fiber, which might be associated with a selective high demand of fiber type I on convexity [18,22].

Combined with the aforementioned findings, the fiber type-specific pathological changes on the concave side seemed to be more severe relative to the contralateral side and the control group. Although bilateral PSM asymmetry in AIS has been found in multiple studies [2,5,7,8,11,13,23], studies comparing the bilateral pathological changes with control subjects are limited. Using MRI, Yeung et al. [2] found significantly higher multifidus signal intensity on concavity in AIS than in control individuals. Additionally, the muscle signal intensity was positively correlated with scoliotic curve. Zapata et al. [24] performed ultrasonographic measurements in mild AIS and found PSM in concavity was significantly thicker than in the control. Stetkarova et al. [8] observed abnormal numerical increases of type I fiber on convexity and type II fiber on concavity compared with a control, while the progression of the Cobb angle



was correlated with the increased fiber type I on convexity. In addition, they found more active electromyography on convexity, which was also demonstrated by Farahpour et al. [10]. Since dynamic postural control is primarily provided by fiber type I, its predominance on the convex side was in line with the finding of more active convex muscle electromyographic activity during dynamic postural control [8,15]. Overall, these studies drew different conclusions concerning the side of abnormality, which might be due to different evaluation methods and nonstringent controls. As for the current study, type-specific morphological and cellular characteristics were comprehensively evaluated, and strict controls were in place: (1) there was no significant demographic difference between AIS and control group; and (2) all the muscle samples were harvested from bilateral thoracic multifidus muscles from T7 to T10 during surgery.

The current study also revealed positive correlations between curve severity (Cobb angle and AVT) and some fiber type-specific morphological/cellular characteristics (CSA, myonuclei density, total/activated SC density) in AIS, especially for type I fiber. Thus, these characteristics could be considered markers for deformity severity. We assumed that the reduced stretch and activity level on concavity could be related to disuse for both muscle fiber types [25].

The findings of the current study can serve as guidance for therapeutic improvement of AIS. Since associations between morphological/cellular characteristics and curve severity have been demonstrated, specific physical therapy for PSM may be of great importance. It is worth noting that the concave side seemed to be more severely affected, especially for fiber type I. Thus, greater attention should be paid to the concave side during PSM physiotherapy treatment to prevent or slow curve progression. Long-duration and high-volume endurance type exercises not only help fiber type transformation from type II to type I, but also contribute to improving the function of fiber type I [26,27]. Therefore, muscle-strengthening exercises on the concavity that concentrate on the sustained

contraction of PMS are recommended. In fact, the aforementioned treatment strategy is an important part of our physiotherapeutic exercise system, which has been shown to be feasible and effective [28].

This study has some limitations. First, the sample size was relatively small. Second, histological evaluation was only performed for a limited portion of the harvested multifidus, which may not have been representative of the whole muscle. In addition, because this was an observational study, it was difficult to ascertain the causality or to determine whether the observed pathological changes were primary or secondary to the scoliotic deformity. Furthermore, if muscle samples from congenital scoliosis were also included as controls, additional information could be obtained to recognize the pathological mechanism of AIS more deeply and comprehensively. Thus, we suggest performing future studies with larger sample sizes to compare the bilateral PSM difference in AIS, congenital scoliosis, and nonscoliosis groups.

## Conclusions

The fiber type-specific pathological changes on the concave side in AIS seemed to be more severe. Some fiber type-specific characteristics (CSA, myonuclei density, total/activated SC density) were closely associated with curve severity. More attention should be paid to PSM physiotherapy treatment on the concave side.

## Acknowledgments

We acknowledge all the participants in this study. In addition, Shao Xiexiang wants to express his special appreciation to Zhou Yu for her endless love, care, and encouragement.

## Conflict of interest

None.

## References:

1. Sarwark JF, Castelein RM, Maqsood A, Aubin CE: The biomechanics of induction in adolescent idiopathic scoliosis: Theoretical factors. *J Bone Joint Surg Am*, 2019; 101(6): e22
2. Yeung KH, Man GCW, Shi L et al: Magnetic resonance imaging-based morphological change of paraspinal muscles in girls with adolescent idiopathic scoliosis. *Spine (Phila Pa 1976)*, 2019; 44(19): 1356–63
3. Dunn J, Henrikson NB, Morrison CC et al: Screening for adolescent idiopathic scoliosis: Evidence report and systematic review for the US Preventive Services Task Force. *JAMA*, 2018; 319(2): 173–87
4. Cheng JC, Castelein RM, Chu WC et al: Adolescent idiopathic scoliosis. *Nat Rev Dis Primers*, 2015; 1: 15030
5. Liu Y, Pan A, Hai Y et al: Asymmetric biomechanical characteristics of the paravertebral muscle in adolescent idiopathic scoliosis. *Clin Biomech (Bristol, Avon)*, 2019; 65: 81–86
6. Wajchenberg M, Astur N, Fernandes EA et al: Assessment of fatty infiltration of the multifidus muscle in patients with adolescent idiopathic scoliosis through evaluation by magnetic resonance imaging compared with histological analysis: A diagnostic accuracy study. *J Pediatr Orthop B*, 2019; 28(4): 362–67
7. Jiang H, Yang F, Lin T et al: Asymmetric expression of H19 and ADIPOQ in concave/convex paravertebral muscles is associated with severe adolescent idiopathic scoliosis. *Mol Med*, 2018; 24(1): 48
8. Stetkarova I, Zamecnik J, Bocek V et al: Electrophysiological and histological changes of paraspinal muscles in adolescent idiopathic scoliosis. *Eur Spine J*, 2016; 25(10): 3146–53
9. Wajchenberg M, Martins DE, de Paiva Luciano R et al: Histochemical analysis of paraspinal rotator muscles from patients with adolescent idiopathic scoliosis: A cross-sectional study. *Medicine*, 2015; 94(8): e598

10. Farahpour N, Younesian H, Bahrpeyma F: Electromyographic activity of erector spinae and external oblique muscles during trunk lateral bending and axial rotation in patients with adolescent idiopathic scoliosis and healthy subjects. *Clin Biomech (Bristol, Avon)*, 2015; 30(5): 411–17
11. Jiang J, Meng Y, Jin X et al: Volumetric and fatty infiltration imbalance of deep paravertebral muscles in adolescent idiopathic scoliosis. *Med Sci Monit*, 2017; 23: 2089–95
12. Mannion AF, Meier M, Grob D, Muntener M: Paraspinal muscle fibre type alterations associated with scoliosis: An old problem revisited with new evidence. *Eur Spine J*, 1998; 7(4): 289–93
13. Gonyea WJ, Moore-Woodard C, Moseley B et al: An evaluation of muscle pathology in idiopathic scoliosis. *J Pediatr Orthop*, 1985; 5(3): 323–29
14. Kim JA, Roy RR, Zhong H et al: PPARdelta preserves a high resistance to fatigue in the mouse medial gastrocnemius after spinal cord transection. *Muscle Nerve*, 2016; 53(2): 287–96
15. Bylund P, Jansson E, Dahlberg E, Eriksson E: Muscle fiber types in thoracic erector spinae muscles. Fiber types in idiopathic and other forms of scoliosis. *Clin Orthop Relat Res*, 1987; (214): 222–28
16. Lam GC, Hill DL, Le LH et al: Vertebral rotation measurement: A summary and comparison of common radiographic and CT methods. *Scoliosis*, 2008; 3: 16
17. Fry CS, Porter C, Sidossis LS et al: Satellite cell activation and apoptosis in skeletal muscle from severely burned children. *J Physiol*, 2016; 594(18): 5223–36
18. Arentson-Lantz EJ, English KL, Paddon-Jones D, Fry CS: Fourteen days of bed rest induces a decline in satellite cell content and robust atrophy of skeletal muscle fibers in middle-aged adults. *J Appl Physiol*, 2016; 120(8): 965–75
19. Petrella JK, Kim JS, Mayhew DL et al: Potent myofiber hypertrophy during resistance training in humans is associated with satellite cell-mediated myonuclear addition: A cluster analysis. *J Applied Physiol*, 2008; 104(6): 1736–42
20. Hogendoorn S, Duijnsveld BJ, van Duinen SG et al: Local injection of autologous bone marrow cells to regenerate muscle in patients with traumatic brachial plexus injury: A pilot study. *Bone Joint Res*, 2014; 3(2): 38–47
21. Kadi F, Ponsot E: The biology of satellite cells and telomeres in human skeletal muscle: Effects of aging and physical activity. *Scand J Med Sci Sports*, 2010; 20(1): 39–48
22. Fry CS, Lee JD, Jackson JR et al: Regulation of the muscle fiber microenvironment by activated satellite cells during hypertrophy. *FASEB J*, 2014; 28(4): 1654–65
23. Mannion AF, Dumas GA, Cooper RG et al: Muscle fibre size and type distribution in thoracic and lumbar regions of erector spinae in healthy subjects without low back pain: Normal values and sex differences. *J Anat*, 1997; 190(Pt 4): 505–13
24. Zapata KA, Wang-Price SS, Sucato DJ, Dempsey-Robertson M: Ultrasonographic measurements of paraspinal muscle thickness in adolescent idiopathic scoliosis: A comparison and reliability study. *Pediatr Phys Ther*, 2015; 27(2): 119–25
25. Uthoff HK, Coletta E, Trudel G: Intramuscular fat accumulation and muscle atrophy in the absence of muscle retraction. *Bone Joint Res*, 2014; 3(4): 117–22
26. Deschenes MR, Maresh CM, Armstrong LE et al: Endurance and resistance exercise induce muscle fiber type specific responses in androgen binding capacity. *J Steroid Biochem Mol Biol*, 1994; 50(3–4): 175–79
27. Wilson JM, Loenneke JP, Jo E et al: The effects of endurance, strength, and power training on muscle fiber type shifting. *J Strength Cond Res*, 2012; 26(6): 1724–29
28. Liu D, Huang S, Yu X et al: Effects of specific exercise therapy on adolescent patients with idiopathic scoliosis: A prospective controlled cohort study. *Spine (Phila Pa 1976)*, 2020 [Online ahead of print]